THE WELL-ALIGNED ORBIT OF WASP-84b: EVIDENCE FOR DISC MIGRATION[†]

D. R. Anderson[1], A. H. M. J. Triaud[2], O. D. Turner[1], D. J. A. Brown[3,4], B. J. M. Clark[1], B. Smalley[1],
A. Collier Cameron[5], A. P. Doyle[1], M. Gillon[6], C. Hellier[1], C. Lovis[7], P. F. L. Maxted[1], D. Pollacco[3],
D. Queloz[7,8], A. M. S. Smith[9,1],

[1] Astrophysics Group, Keele University, Staffordshire ST5 5BG, UK
[2] Department of Physics, and Kavli Institute for Astrophysics and Space Research, MIT, Cambridge, MA 02139, USA
[3] Department of Physics, University of Warwick, Coventry CV4 7AL, UK
[4] Astrophysics Research Centre, School of Mathematics & Physics, Queen's University, University Road, Belfast BT7 1NN
[5] SUPA, School of Physics and Astronomy, University of St. Andrews, North Haugh, Fife KY16 9SS, UK
[6] Institut d'Astrophysique et de Géophysique, Université de Liège, Allée du 6 Août, 17, Bat. B5C, Liège 1, Belgium
[7] Observatoire de Genève, Université de Genève, 51 Chemin des Maillettes, 1290 Sauverny, Switzerland
[8] Cavendish Laboratory, J J Thomson Avenue, Cambridge, CB3 0HE, UK
[9] N. Copernicus Astronomical Centre, Polish Academy of Sciences, Bartycka 18, 00-716, Warsaw, Poland

Draft version September 24, 2014

ABSTRACT

We report the sky-projected orbital obliquity (spin-orbit angle) of WASP-84b, a 0.70-$M_{\rm Jup}$ planet in a 8.52-day orbit around a G9V/K0V star, to be $\lambda = 0.3 \pm 1.7°$. We obtain a true obliquity of $\psi = 14.8 \pm 8.0°$ from a measurement of the inclination of the stellar spin axis with respect to the sky plane. Due to the young age and the weak tidal forcing of the system, we suggest that the orbit of WASP-84b is unlikely to have both realigned and circularised from the misaligned and/or eccentric orbit likely to have arisen from high-eccentricity migration. Therefore we conclude that the planet probably migrated via interaction with the protoplanetary disc. This would make it the first short-orbit, giant planet to have been shown to have migrated via this pathway. Further, we argue that the distribution of obliquities for planets orbiting cool stars ($T_{\rm eff} < 6250$ K) suggests that high-eccentricity migration is an important pathway for the formation of short-orbit, giant planets.

Subject headings: planets and satellites: dynamical evolution and stability — planet-disk interactions — planet-star interactions — planets and satellites: individual: WASP-84b — stars: individual: WASP-84

1. INTRODUCTION

The orbital obliquity (spin-orbit angle; ψ) distribution of short-orbit, giant planets, or "hot Jupiters", may be indicative of the manner in which they arrived in their current orbits from farther out, where they presumably formed (e.g. Rafikov 2006). As a star and its planet-forming disc both inherit their angular momenta from their parent molecular cloud, stellar spin and planetary orbital axes are expected to be, at least initially, aligned ($\psi = 0$). Migration via interaction with the gas disc is expected to preserve this initial spin-orbit alignment (Lin et al. 1996; Marzari & Nelson 2009). Migration via high-eccentricity migration, in which a cold Jupiter is perturbed into an eccentric, misaligned orbit that is then circularised, shortened and realigned by tidal dissipation, is expected to produce a broad range of obliquities (Fabrycky & Tremaine 2007; Nagasawa et al. 2008; Matsumura et al. 2010; Naoz et al. 2011).

A broad range of obliquities has been found for hot-star systems ($T_{\rm eff} > 6250$ K), for which tidal realignment is expected to be inefficient due to the absence of a substantial convective envelope (Winn et al. 2010a; Schlaufman

2010), whereas systems with massive stars that had no convective envelope on the main sequence, but that are old enough to have developed convective envelopes ($\gtrsim 2.5$ Gyr), are aligned (Triaud 2011). Conversely, cool-star systems experiencing strong tidal forcing—that is those with short scaled semi-major axes, a/R_*, and high planet-to-star mass ratios—tend to be aligned (see Albrecht et al. 2012 and references therein). The obliquities of nine planets orbiting cool stars and experiencing weak tidal forcing ($a/R_* > 15$) have been measured: HAT-P-11b, (Winn et al. 2010b; Hirano et al. 2011a; Sanchis-Ojeda & Winn 2011), HAT-P-17b (Fulton et al. 2013), HAT-P-18b (Esposito et al. 2014), HD 17156 b (Narita et al. 2008; Cochran et al. 2008; Barbieri et al. 2009; Narita et al. 2009), HD 80606 b (Moutou et al. 2009; Pont et al. 2009; Winn et al. 2009; Hébrard et al. 2010), Kepler-30b (Sanchis-Ojeda et al. 2012), Kepler-63b (Sanchis-Ojeda et al. 2013), WASP-8b (Queloz et al. 2010) and WASP-117b (Lendl et al. 2014). The orbits of all but HD 17156 b and, possibly, HAT-P-17b are misaligned and all but HAT-P-18b and Kepler-63b are eccentric.

Various groups are attempting to reproduce the observed obliquity distribution with models (e.g. Naoz et al. 2012; Rogers & Lin 2013; Xue et al. 2014; Dawson 2014). We require a larger sample of measured obliquities, especially for weak-tide, cool-star systems, and more realistic models to be able to discern the relative contribution of the different migration pathways and to better understand the physical processes

involved in tidal dissipation and orbital realignment. Here we present an obliquity measurement for the weak-tide, cool-star system WASP-84 from observations of its Rossiter-McLaughlin (RM) effect (e.g. Albrecht et al. 2012). Anderson et al. (2013, hereafter A13) found the WASP-84 system to comprise a 0.69-$M_{\rm Jup}$ planet in a circular ($e < 0.077$ at $2\,\sigma$), 8.52-d orbit around an active K0V star.

2. OBSERVATIONS

We obtained 17 spectra of WASP-84 with HARPS on the ESO 3.6-m telescope (Pepe et al. 2002) through the transit of 2013 Feb 4–5 and a further 13 spectra around the orbit. The transit spectra, with exposure times of 1200 s, were taken over an airmass range of 1.39–1.17–1.92 and have signal-to-noise ratio (SNR) of 19–40 per pixel at 5500Å. The seeing deteriorated to $>2''$ going into the transit, which reduced the flux entering the fibre. We chose to switch the read-out mode from fast to slow for the final 6 spectra, aiming for a higher precision at the expense of time resolution. The Moon, 31 per cent illuminated and 115° from WASP-84, rose at the time of mid-transit. The spectra around the orbit had exposure times of 600 s, except for the final spectrum, for which the exposure time was 900 s.

We obtained 38 spectra of WASP-84 with HARPS-North on the 3.6-m Telescopio Nazionale Galileo (Cosentino et al. 2012) through the transit of 2014 Jan 11–12. There was light cloud throughout the night, though it cleared during the latter portion of the sequence. At the time of mid-transit the Moon was 85 per cent illuminated at a distance of 66° from WASP-84. We discarded the final 5 spectra as they were taken when the target was significantly beyond an airmass of 2 and the final spectrum was aborted. The remaining 33 spectra, each with an exposure time of 600 s, covered an airmass range of 1.27–1.12–2.06 and have SNR of 25–42 per pixel at 5500Å.

We used the HARPS pipeline to process the HARPS and HARPS-North spectra and to compute radial velocities (RVs) by weighted cross-correlation with a numerical K5-spectral template (Pepe et al. 2005).

Concurrently with HARPS-North, we observed WASP-84 during the same transit and from the same site with the RISE fast-readout photometer mounted on the 2-m Liverpool Telescope (Steele et al. 2008). RISE has a single fixed $V+R$ filter, a field of view of $9'.2 \times 9'.2$ and zero read-out overhead. We defocussed the instrument and used autoguiding to minimise the effect of flat-fielding errors. We used an exposure time of 4 s to acquire 4236 images. Over the sequence the airmass of the target ranged over 1.12–1.80. We performed differential aperture photometry on the images using 5 comparison stars.

We plot the HARPS and HARPS-North RVs and the RISE photometry obtained through the transit in Figure 1 and all the RVs around the orbit in Figure 2. Time-correlated noise is evident in the early portion of the transit in both the HARPS and the HARPS-North RV sequences. We suggest that this results from a meteorological coincidence rather than being due to an astrophysical source: the seeing deteriorated at the start of the transit observed by HARPS, which resulted in a drop in SNR; and the scatter in the HARPS-North RVs correlates well with the cloud visible in the Liverpool Telescope's sky cameras[2].

3. STELLAR PARAMETERS FROM THE HARPS SPECTRA

We coadded the individual HARPS spectra to produce a single spectrum with an average signal-to-noise ratio of 100:1. We performed the spectral analysis using the methods detailed in Doyle et al. (2013). The excitation balance of the Fe I lines was used to determine the effective temperature ($T_{\rm eff}$). The surface gravity ($\log g_*$) was determined from the ionisation balance of Fe I and Fe II and using the Na I D lines. The iron abundance was obtained from equivalent width measurements of 47 unblended Fe I and Fe II lines. The quoted error estimates include that given by the uncertainties in $T_{\rm eff}$ and $\log g_*$, as well as the scatter due to measurement and atomic data uncertainties. The projected stellar rotation velocity ($v_* \sin I_*$) was determined by fitting the profiles of several unblended Fe I lines in the wavelength range 6000–6200Å. A value for macroturbulent velocity of 2.13 $\pm$ 0.73 km s^{-1} was assumed from the asteorseismic-based calibration of Doyle et al. (2014). Using those spectra with SNR > 20 and assuming $B - V = 0.82$, we determined the $\log R'_{\rm HK}$ activity index from the emission in the cores of the Ca II H+K lines (e.g. Boisse et al. 2009). The results of the spectral analysis are given in Table 1.

4. OBLIQUITY AND SYSTEM PARAMETERS FROM THE HARPS RADIAL VELOCITIES AND THE RISE LIGHTCURVES

We determined the sky-projected obliquity and the system parameters from a simultaneous fit to the transit lightcurves and the radial velocities. The fit was performed using the current version of the Markov-chain Monte Carlo (MCMC) code described by Collier Cameron et al. (2007) and Anderson et al. (2014). The RM effect was modelled using the formulation of Hirano et al. (2011b).

The available time-series photometry on WASP-84 are: the WASP lightcurves spanning 2009 Jan–2011 Apr (A13); a partial-transit lightcurve from TRAPPIST (A13); two full-transit lightcurves from RISE (A13); and a third RISE lightcurve (this paper). The available RV data are: 20 CORALIE RVs around the orbit, pre-whitened for stellar activity using a simple harmonic series (A13); and 13 HARPS spectra around the orbit, 17 HARPS spectra through a transit, and 38 HARPS-North spectra through a transit (this paper). Unlike with the CORALIE RVs, we found no reason to pre-whiten the HARPS orbital RVs: the Pearson correlation coefficient between residual RV and bisector span is $r = -0.23$ for the 13 RVs; this becomes $r = 0.04$ when excluding the latest RV, which was taken the season after the other 12 measurements. This compares with $r = -0.71$ for the 20 CORALIE RVs (A13).

In our final MCMC analysis we opted to determine the system parameters using only the three high-quality

---

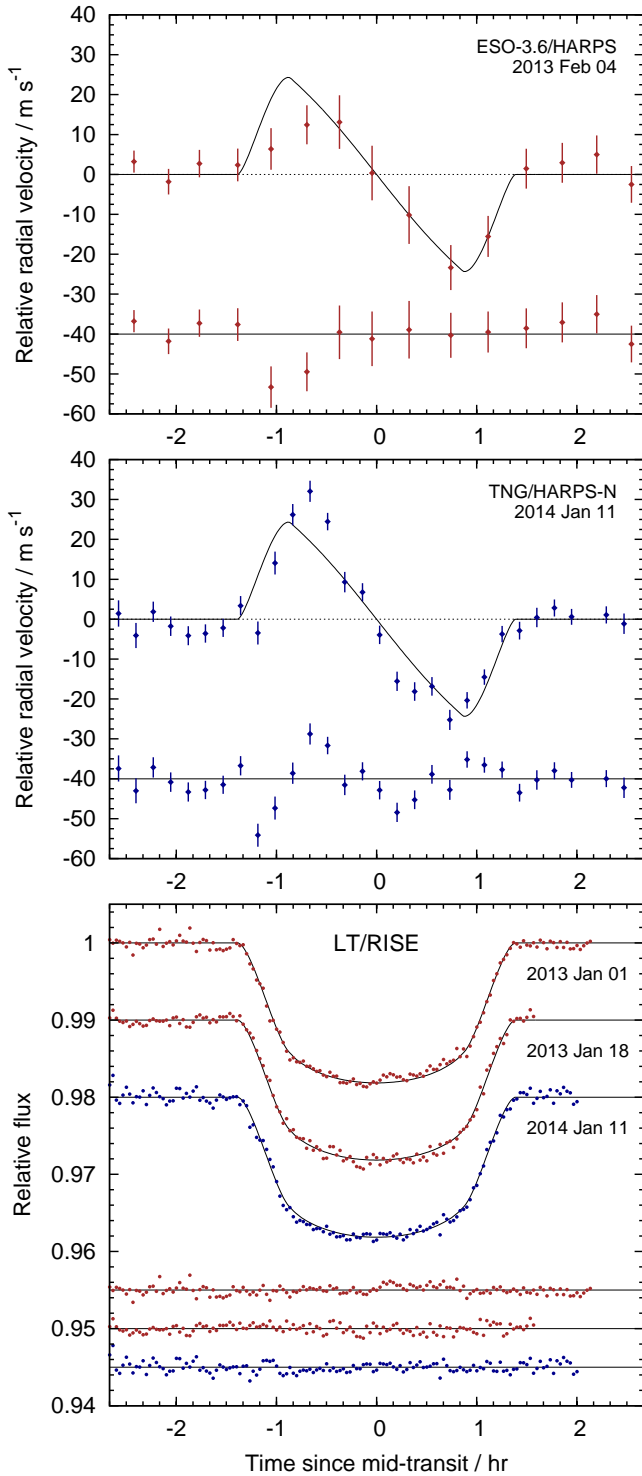[2] http://telescope.livjm.ac.uk/Reports - see especially the "SkyCam-T" video.

FIG. 1.— *Top panel:* The HARPS radial velocities with the best-fitting Rossiter-McLaughlin effect. The circular Keplerian model has been subtracted. The seeing deteriorated going into the transit. *Middle panel:* The HARPS-North radial velocities with the best-fitting Rossiter-McLaughlin effect. The circular Keplerian model has been subtracted. The time-correlated noise correlates with cloud. *Bottom panel:* LT/RISE transit lightcurves presented in A13 (top two lightcurves) and herein (bottom lightcurve), offset for clarity and binned with a bin width of two minutes. The best-fitting transit model is superimposed. The residuals about the model are plotted below the lightcurves in the same order. The planet appears to have crossed an active region shortly after mid-transit during the transit of 2013 Jan 01, which was a photometric night. The same may have happened during the ingress of the transit of 2014 Jan 11, though there was light cloud that night.
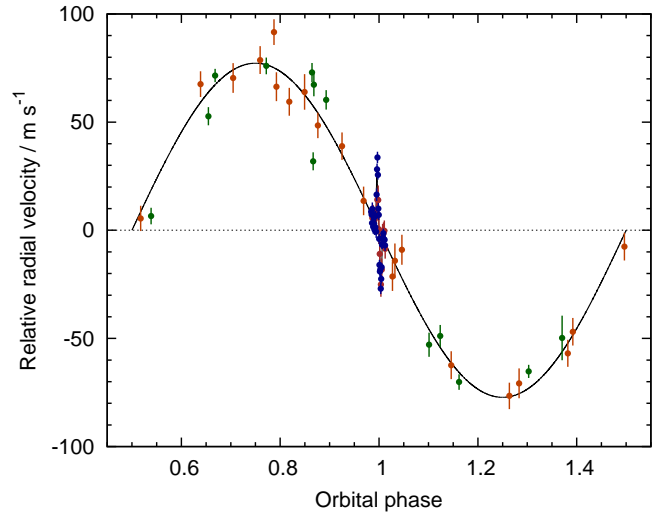

FIG. 2.— The radial velocities from CORALIE (pre-whitened; orange symbols; A13), HARPS (green symbols for the orbit, brown for the transit; this paper) and HARPS-North (blue symbols; this paper). The best-fitting circular Keplerian and RM model is superimposed.

RISE lightcurves and all the RVs, which were partitioned as listed above to allow for instrumental and astrophysical offsets. The excluded WASP photometry was imperfectly detrended for rotational modulation and instrumental noise and the excluded TRAPPIST photometry covers only the first half of the transit and was obtained at high airmass (1.47 at ingress to 2.40 at the end of the observation). We included the timing information of the WASP and TRAPPIST photometry in our final analysis by placing a normal prior on the time of mid-transit ($T_0 = 2\,456\,439.52878 \pm 0.00015$ d), which was the T_0 from an initial anlysis including all the listed data, but with an error bar larger by a factor of 2 to account for the double-weighting of the remaining photometry.

The stellar density reported in A13 ($\rho_* = 2.02 \pm 0.07\,\rho_\odot$) seemed high a star of the reported mass ($0.84 \pm 0.04\,M_\odot$), which was determined from an empirical mass calibration. As a consistency check, we opted to determine stellar mass from a comparison with stellar models. We determined $\rho_* = 1.851 \pm 0.049\,\rho_\odot$ from an initial analysis that omitted the WASP and TRAPPIST data. We input that value of ρ_* and the values of $T_{\rm eff}$ and [Fe/H] from the spectral analysis into the BAGEMASS stellar evolution MCMC code of Maxted et al. (2014), from which we obtained a stellar mass of $M_* = 0.855 \pm 0.028$ $M_\odot$ and a stellar age of 2.0 ± 1.6 Gyr. In our final analysis, we drew a value of M_* at each MCMC step from a normal distribution with mean and standard deviation equal to the BAGEMASS-derived values, but with an error bar larger by a factor 2 to allow for uncertainties due to the unknown helium abundance and the effects of magnetic activity on the mass-radius relation; thus we had no need of a mass calibration.

In our final analysis, we adopted a circular orbit, which Anderson et al. (2012) advocate is the prudent choice for hot Jupiters in the absence of evidence to the contrary. In an initial analysis, in which we fit for eccentricity, e, we found $e = 0.018 \pm 0.011$ and $e < 0.041$ at the 2-σ level.

The median values and the 1-σ limits of our MCMC

parameters' posterior distributions are given in Table 1. The best fits to the radial velocities and the photometry are plotted in Figures 1 and 2. The presented solution supersedes that of the discovery paper owing to the additional RISE lightcurve and HARPS RVs, and the omission of the lower-quality WASP and TRAPPIST lightcurves.

We obtained $\lambda = 0.3 \pm 1.7°$ and $v_* \sin I_* = 2.593 \pm 0.087$ km s^{-1} when fitting the RM effect to both the HARPS-North and HARPS RVs. Unsurprisingly, the HARPS-North RVs, with both a cadence and a typical precision twice that of the HARPS RVs, do most to constrain the RM effect: we obtained $\lambda = -0.9 \pm 1.6°$ and $v_* \sin I_* = 2.650 \pm 0.089$ km s^{-1} when using only the HARPS-North RVs, and we obtained $\lambda = 11.6 \pm 7.5°$ and $v_* \sin I_* = 1.96 \pm 0.31$ km s^{-1} when using only the HARPS RVs. Primarily due to the omission of the WASP photometry, we obtained a lower stellar density as compared to the discovery paper ($1.89 \pm 0.05 \, \rho_\odot$ cf. $2.02 \pm 0.07 \, \rho_\odot$; A13).

5. RESULTS AND DISCUSSION

We find the sky-projected spin-orbit angle, or projected obliquity, of WASP-84b to be $\lambda = 0.3 \pm 1.7°$. With a measurement of the angle between the stellar spin axis and the line of sight, I_*, we can calculate the true obliquity, ψ, using equation 9 of Fabrycky & Winn (2009)). Using the stellar rotation period of $P_{\rm rot} = 14.36 \pm 0.35$ d, derived by A13 from observed photometric modulation, and our MCMC posterior distributions of R_*, $v_* \sin I_*$ $i_{\rm P}$ and λ, we calculate $v_* = 2.70 \pm 0.09$ km s^{-1}, $I_* = 73.5°$ ($I_* > 70.0°$ at the 1-σ level), and $\psi = 14.8 \pm 8.0°$; these are our adopted values. This is consistent with a well-aligned orbit and certainly excludes polar or retrograde orbits as observed for some other hot-Jupiter systems. We obtained consistent results from analyses using: only the HARPS-North RVs ($I_* = 78.5°$, $I_* > 73.4°$ at 1σ; $\psi = 10.0 \pm 7.6°$); only the HARPS RVs ($I_* = 46.8°$, $I_* > 42.2°$ at 1σ; $\psi = 43 \pm 10°$); all the RVs and the spectral $v_* \sin I_*$ ($I_* = 90.0°$, $I_* > 68.7°$ at 1σ; $\psi = 3 \pm 18°$). Using the relation between $P_{\rm rot}$ and $\log R'_{\rm HK}$ of Mamajek & Hillenbrand (2008), we obtained $P_{\rm rot} = 11.4 \pm 1.7$ d, which is consistent with the $P_{\rm rot}$ from photometric modulation.

We found the orbital eccentricity of WASP-84b to be low and consistent with a circular orbit: $e = 0.018 \pm 0.011$ and $e < 0.041$ at the 2-σ level. Using the $\log R'_{\rm HK}$ age-activity relation of Mamajek & Hillenbrand (2008) we obtained an age of 0.70 ± 0.18 Gyr. This compares with our evolutionary-analysis age of 2.1 ± 1.6 Gyr (Section 4) and the gyrochronolgical ages of 0.8 ± 0.1 Gyr and ~ 1.4 Gyr from A13. Using equation 2 of Albrecht et al. (2012) we calculate the relative timescale for alignment via tidal dissipation to be 4.2×10^{14} yr.

Considering the young age and the weak tidal forcing of the WASP-84 system, we suggest that it is improbable that the orbit of WASP-84b could have circularised and re-aligned from the eccentric, misaligned orbit likely to have arisen from migration via a high-eccentricity pathway. We suggest that WASP-84b probably migrated to its current 8.52-d orbit via interaction with the protoplanetary disc. This would make it the first short-orbit, giant planet to have been shown to have done so.

Another candidate for disc migration is HAT-P-17b,

Parameter, Symbol / Unit	Value
Spectral analysis:	
Stellar effective temperature, $T_{\rm eff}$ / K	5280 ± 80
Stellar surface gravity, $\log g_*$ / (cgs)	4.65 ± 0.17
Stellar metallicity, [Fe/H]	$+0.09 \pm 0.12$
Microturbulence, $\xi_{\rm t}$ / km s^{-1}	0.7 ± 0.3
Macroturbulence[a], $v_{\rm mac}$ / km s^{-1}	2.13 ± 0.73
Proj. stellar rot. vel., $v_* \sin I_*$ / km s^{-1}	2.9 ± 0.8
Lithium abundance, $\log A({\rm Li})$	<0.7
Ca II H+K activity index, $\log R'_{\rm HK}$	-4.44
MCMC proposal parameters:	
Period, P / d	8.5234964 ± 0.0000036
Mid-transit[b], T_0 / d	6448.052287 ± 0.000067
Transit duration, T_{14} / d	0.11536 ± 0.00039
Transit depth, $\Delta F = R_{\rm P}^2/R_*^2$	0.01705 ± 0.00011
Impact parameter, b	0.6534 ± 0.0084
Reflex velocity, K_1 / m s^{-1}	77.2 ± 2.1
Systemic velocity, γ / m s^{-1}	$-11\,578.2 \pm 1.5$
HARPS-North offset, $\gamma_{\rm off,N,tran}$ / m s^{-1}	-21.50 ± 0.50
HARPS transit offset, $\gamma_{\rm off,S,tran}$ / m s^{-1}	28.24 ± 0.71
HARPS orbital offset, $\gamma_{\rm off,S,orb}$ / m s^{-1}	14.00 ± 0.44
$\sqrt{v_* \sin I} \cos \lambda$	1.610 ± 0.027
$\sqrt{v_* \sin I} \sin \lambda$	0.001 ± 0.047
eccentricity, e	0 (adopted; <0.041 at 2σ)
MCMC derived parameters:	
Projected orbital obliquity, λ / °	0.3 ± 1.7
Orbital obliquity[c], ψ / °	14.8 ± 8.0
Proj. stellar rot. vel., $v_* \sin I_*$ / km s^{-1}	2.593 ± 0.087
Stellar rotation velocity[b], v_* / km s^{-1}	2.70 ± 0.09
Stellar spin inclination[b], I_* / °	73.5 (> 70.0 at 1σ)
Orbital inclination, $i_{\rm P}$ / °	88.275 ± 0.037
Scaled orbital separation, a/R_*	21.70 ± 0.19
Ingress/egress duration, $T_{12} (= T_{34})$ / d	0.02181 ± 0.00048
Stellar mass, M_* / $M_\odot$	0.854 ± 0.057
Stellar radius, R_* / $R_\odot$	0.768 ± 0.018
Stellar surface gravity, $\log g_*$ / (cgs)	4.598 ± 0.012
Stellar density, ρ_*	1.886 ± 0.050
Planetary mass, $M_{\rm P}$	0.700 ± 0.037
Planetary radius, $R_{\rm P}$	0.975 ± 0.025
Planetary surface gravity, $\log g_{\rm P}$ / (cgs)	3.226 ± 0.016
Planetary density, $\rho_{\rm P}$ / $\rho_{\rm Jup}$	0.755 ± 0.038
Orbital major semi-axis, a / au	0.0775 ± 0.0017
Planetary equilib. temperat., $T_{\rm eql}$ / K	832 ± 13

[a] $v_{\rm mac}$ value obtained using the calibration of Doyle et al. (2014).
[b] T_0 is in HJD (UTC) and 2 450 000 has been subtracted.
[c] See Section 5 for the calculation of ψ, v_* and I_*.

which has a slightly larger scaled semi-major axis ($a/R_* = 22.6$ cf. 21.6) and a slightly smaller mass ratio ($M_{\rm P}/M_* = 0.00059$ cf. 0.00078). Though HAT-P-17b may be aligned ($\lambda = 19 \pm 15°$), Fulton et al. (2013) find that the data weakly favour a misaligned orbit. Further, the orbit is eccentric ($e = 0.342 \pm 0.006$) and the system is old (7.8 ± 3.3 Gyr; Howard et al. 2012). Thus the evidence for disc migration is less compelling.

6. THE DEPENDENCE OF ALIGNMENT ON ORBITAL DISTANCE

A broad range of obliquities has been found for hot-star systems ($T_{\rm eff} > 6250$ K), whereas cool-star systems tend to be aligned. This has been interpreted as evidence for realignment by tidal dissipation, which is suggested to be efficient for cool stars with their deep convections layers and inefficient for hot stars that lack substantial convective envelopes (Winn et al. 2010a; Schlaufman

2010). For viscous dissipation in a convective layer, the timescale for spin-orbit alignment is proportional to both the sixth power of the scaled orbital separation, $(a/R_*)^6$, and the square of the star-to-planet mass ratio, $(M_*/M_P)^2$, (Zahn 1977). Thus, if short-orbit, giant planets migrate via high-eccentricty pathways and realign via tidal dissipation then, for cool stars, there should be a trend from spin-orbit alignment for close-in planets to a broad range of obliquities for those in more distant orbits.

We selected those cool-star systems with $T_{\rm eff} \leq 6150$ K (to account for uncertainties) and with a mean uncertainty on λ less than $20°$. Their spin-orbit angles are plotted in Figure 3, as a function of orbital distance in units of stellar radii $a/R_\star$, which is determined directly from the depth and width of the transit lightcurve (Seager & Mallén-Ornelas 2003). We see that λ is confined to within $\sim 20°$ of aligned at orbital separations of $\lesssim 15$ stellar radii and that the distribution is broad at greater separations. No such pattern is observed for hot stars, which exhibit a broad distribution of λ at $a/R_\star < 15$. This suggests that a high fraction of hot Jupiters orbiting cool stars used to be misaligned and that tides changed that initial distribution either by realigning the orbits or by destroying misaligned planets.

6.1. Giant-planet migration

We note that orbits shorter than $a/R_\star < 15$ are circular, whereas longer orbits are often eccentric (Figure 3). As tides become ineffective with sufficient distance from the star, the population that we are beginning to see at $a/R_\star > 15$ may be close to the initial distribution in spin-orbit angle. The misaligned and/or eccentric systems are suggestive of high-eccentricity migration and the aligned, circular system of WASP-84 is suggestive of disc-driven migration. Thus both pathways appear to factor in the inward migration of giant planets; by measuring more systems in the weak-tide regime we can determine their relative contributions.

ACKNOWLEDGEMENTS

REFERENCES

Albrecht, S., Winn, J. N., Johnson, J. A., et al. 2012, ApJ, 757, 18
Anderson, D. R., Collier Cameron, A., Gillon, M., et al. 2012, MNRAS, 422, 1988
Anderson, D. R., Collier Cameron, A., Delrez, L., et al. 2013, MNRAS, in press, arXiv:1310.5654
Anderson, D. R., Collier Cameron, A., Hellier, C., et al. 2014, A&A, submitted, arXiv:1402.1482
Barbieri, M., Alonso, R., Desidera, S., et al. 2009, A&A, 503, 601
Boisse, I., Moutou, C., Vidal-Madjar, A., et al. 2009, A&A, 495, 959
Cochran, W. D., Redfield, S., Endl, M., & Cochran, A. L. 2008, ApJ, 683, L59
Collier Cameron, A., Wilson, D. M., West, R. G., et al. 2007, MNRAS, 380, 1230
Cosentino, R., Lovis, C., Pepe, F., et al. 2012, in Society of Photo-Optical Instrumentation Engineers (SPIE) Conference Series, Vol. 8446, Society of Photo-Optical Instrumentation Engineers (SPIE) Conference Series
Dawson, R. I. 2014, ApJ, 790, L31
Doyle, A. P., Davies, G. R., Smalley, B., Chaplin, W. J., & Elsworth, Y. 2014, ArXiv e-prints, arXiv:1408.3988
Doyle, A. P., Smalley, B., Maxted, P. F. L., et al. 2013, MNRAS, 428, 3164
Esposito, M., Covino, E., Mancini, L., et al. 2014, A&A, 564, L13
Fabrycky, D., & Tremaine, S. 2007, ApJ, 669, 1298
Fabrycky, D. C., & Winn, J. N. 2009, ApJ, 696, 1230
Fulton, B. J., Howard, A. W., Winn, J. N., et al. 2013, ApJ, 772, 80
Hébrard, G., Désert, J.-M., Díaz, R. F., et al. 2010, A&A, 516, A95
Hirano, T., Narita, N., Shporer, A., et al. 2011a, PASJ, 63, 531
Hirano, T., Suto, Y., Winn, J. N., et al. 2011b, ApJ, 742, 69
Howard, A. W., Bakos, G. Á., Hartman, J., et al. 2012, ApJ, 749, 134
Lendl, M., Triaud, A. H. M. J., Anderson, D. R., et al. 2014, A&A, 568, A81
Lin, D. N. C., Bodenheimer, P., & Richardson, D. C. 1996, Nature, 380, 606
Mamajek, E. E., & Hillenbrand, L. A. 2008, ApJ, 687, 1264
Marzari, F., & Nelson, A. F. 2009, ApJ, 705, 1575
Matsumura, S., Peale, S. J., & Rasio, F. A. 2010, ApJ, 725, 1995
Maxted, P. F. L., Serenelli, A. M., & Southworth, J. 2014, MNRAS, arXiv:astro-ph/0609744
Moutou, C., Hébrard, G., Bouchy, F., et al. 2009, A&A, 498, L5
Nagasawa, M., Ida, S., & Bessho, T. 2008, ApJ, 678, 498

FIG. 3.— The projected obliquity, λ, of planetary orbital planes as a function of scaled orbital distance, $a/R_\star$, for those systems with $T_{\rm eff} \leq 6150$ K and $\overline{\sigma}_\lambda < 20°$. The filled symbols depict near-circular orbits ($e < 0.1$ or e consistent with zero) and the open symbols depict eccentric orbits. WASP-84b is depicted by a blue triangle.

Naoz, S., Farr, W. M., Lithwick, Y., Rasio, F. A., & Teyssandier, J. 2011, Nature, 473, 187
Naoz, S., Farr, W. M., & Rasio, F. A. 2012, ApJ, 754, L36
Narita, N., Sato, B., Ohshima, O., & Winn, J. N. 2008, PASJ, 60, L1
Narita, N., Hirano, T., Sato, B., et al. 2009, PASJ, 61, 991
Pepe, F., Mayor, M., Rupprecht, G., et al. 2002, The Messenger, 110, 9
Pepe, F., Mayor, M., Queloz, D., et al. 2005, The Messenger, 120, 22
Pont, F., Hébrard, G., Irwin, J. M., et al. 2009, A&A, 502, 695
Queloz, D., Anderson, D., Collier Cameron, A., et al. 2010, A&A, 517, L1+
Rafikov, R. R. 2006, ApJ, 648, 666
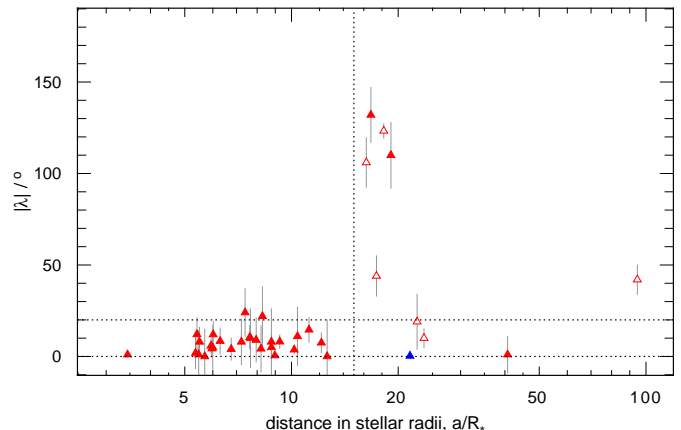Rogers, T. M., & Lin, D. N. C. 2013, ApJ, 769, L10

Sanchis-Ojeda, R., & Winn, J. N. 2011, ApJ, 743, 61
Sanchis-Ojeda, R., Fabrycky, D. C., Winn, J. N., et al. 2012, Nature, 487, 449
Sanchis-Ojeda, R., Winn, J. N., Marcy, G. W., et al. 2013, ApJ, 775, 54
Schlaufman, K. C. 2010, ApJ, 719, 602
Seager, S., & Mallén-Ornelas, G. 2003, ApJ, 585, 1038

Steele, I. A., Bates, S. D., Gibson, N., et al. 2008, in Society of Photo-Optical Instrumentation Engineers (SPIE) Conference Series, Vol. 7014, Society of Photo-Optical Instrumentation Engineers (SPIE) Conference Series
Triaud, A. H. M. J. 2011, A&A, 534, L6
Winn, J. N., Fabrycky, D., Albrecht, S., & Johnson, J. A. 2010a, ApJ, 718, L145
Winn, J. N., Howard, A. W., Johnson, J. A., et al. 2009, ApJ, 703, 2091
Winn, J. N., Johnson, J. A., Howard, A. W., et al. 2010b, ApJ, 723, L223
Xue, Y., Suto, Y., Taruya, A., et al. 2014, ApJ, 784, 66
Zahn, J. 1977, A&A, 57, 383